

# QCD Plasma Instabilities: The Nonabelian Cascade

Peter Arnold

*Department of Physics, University of Virginia,  
Box 400714, Charlottesville, Virginia 22901, USA*

Guy D. Moore

*Department of Physics, McGill University,  
3600 rue University, Montréal QC H3A 2T8, Canada*

(Dated: September 20, 2005)

## Abstract

Magnetic plasma instabilities appear to play an important role in the early stages of quark-gluon plasma equilibration in the high energy (weak coupling) limit. Numerical studies of the growth of such instabilities from small seed fluctuations have found initial exponential growth in their energy, followed by linear growth once the associated color magnetic fields become so large that their non-abelian interaction are non-perturbative. In this paper, we use simulations to determine the nature of this linear energy growth. We find that the long-wavelength modes associated with the instability have ceased to grow, but that they cascade energy towards the ultraviolet in the form of plasmon excitations of ever increasing energy. We find a quasi-steady-state power-law distribution  $f_k \propto k^{-\nu}$  for this cascade, with spectral index  $\nu \simeq 2$ .

## I. INTRODUCTION

One of the surprises which has emerged from the heavy ion experiments at RHIC is that the medium or plasma which is produced in a heavy ion collision appears to display collective behavior analogous to a fluid with a very small viscosity (the so-called “Quark-Gluon Liquid”) [1]. In particular, hydrodynamic treatments taking the medium to be an ideal fluid give the correct flow description [2]. To clarify, we remind the reader that “ideal fluid” is the opposite of “ideal gas”; it means that scatterings or interactions so efficiently maintain local equilibrium (or at least isotropy), that the stress tensor remains everywhere isotropic when measured in the local rest frame. Gases behave like ideal fluids on distance and time scales large compared to transport mean free paths and mean free times.

The most popular, and perhaps most likely, explanation for the small viscosity is that the Quark-Gluon Plasma at the energy densities achieved at RHIC is very far from weak coupling. The strong coupling  $\alpha_s$  is large, interactions are very strong, and the collective behavior is natural. To secure this interpretation, we would need to see that the observed behavior really differs from the expected weakly coupled behavior. Most treatments to date of weakly coupled hot QCD show that equilibration is slow [3] (see however [4]). However, we have recently shown [5] that even the most complete of these, the “bottom-up” scenario of Baier, Mueller, Schiff and Son [6], is incorrect, because it ignores plasma instabilities [7], which in fact dominate the physics of weakly-coupled anisotropic plasmas, in QCD or in ordinary QED.

Plasma instabilities arise as a result of two pieces of physics. First, Lorentz contraction of the nuclei means that the initial region of plasma is a flat pancake shape. It is reasonable to expect at weak coupling that quarks and gluons will for a time fly in nearly straight lines at near the speed of light (at least, once the system has expanded enough that the densities of quarks and gluons are perturbative). Consider particles scattered in all directions in the initial moments of the collision. The starting geometry dictates that the momentum distribution of particles will subsequently become highly anisotropic with time, as illustrated in Fig. 1. Second, in the presence of such anisotropic momentum distributions, certain soft gauge field configurations grow exponentially, at least if they are small enough for a perturbative treatment to be reliable.

Not only have plasma instabilities not been fully taken into account in studying the

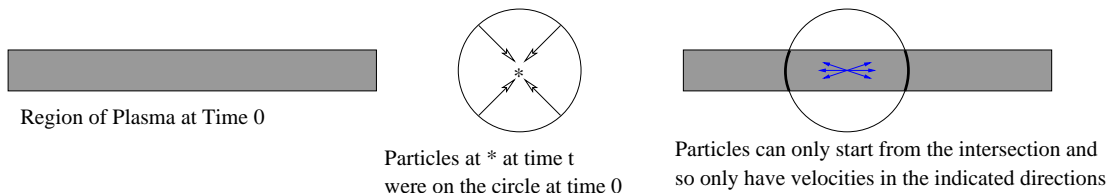


FIG. 1: Cartoon of why the momentum distribution becomes anisotropic. The starting region is thin along the beam axis (vertical in this figure). Since particles fly in a straight line at the speed of light, particles at point  $*$  at time  $t$  originated at time 0 on a sphere of radius  $t$  centered at  $*$ . But only part of this sphere was in the plasma; so only particles with small beam-axis momenta can get to point  $*$  at time  $t$ , and the momentum distribution is anisotropic.

evolution of the Quark-Gluon Plasma; instabilities in Yang-Mills theory in general are not yet well understood or well characterized. Therefore, at the current juncture we cannot say whether the experimental results at RHIC are in contradiction with weakly coupled predictions, because we simply do not know what the predictions of isotropization in a weakly coupled Quark-Gluon Plasma actually are. This rather embarrassing gap in our knowledge needs to be filled. In particular, the behavior of plasma instabilities in a nonabelian theory such as QCD are expected to be intrinsically different from the case of an ordinary QED plasma, because nonabelian gauge fields can directly interact with each other, and because charge carriers can have their colors rotated by intervening QCD fields.

Recently there has been substantial progress on this problem, though it is far from settled. The growth of QCD plasma instabilities when the soft colored gauge fields are small has been well characterized [5, 8]. Arnold and Lenaghan [9] conjectured that exponential growth would continue after QCD fields became large. 1+1 dimensional simulations [10, 11] confirmed this behavior, but 3+1 dimensional studies [12, 13] showed something different: when soft colored gauge fields become large due to instability growth, exponential growth shuts off and the energy in soft gauge fields instead grows *linearly* with time. Recent partial attempts to explore the consequences of instabilities for thermalization may be found in Refs. [14].

The goal of this paper is to further investigate the behavior of an anisotropic quark-gluon plasma, after soft gauge fields have become large. We will show that the soft gauge fields with wave-numbers which should make them unstable instead enter a dynamical quasi-steady state, gaining energy from the instability but losing energy, via their nonabelian interactions, to more ultraviolet field excitations. The energy released into infrared gauge fields by the instability then cascades towards higher wave-number gauge field modes, with occupation number  $f(k) \propto k^{-\nu}$  up to a time-dependent cutoff  $k_{\max}(t)$ . Through simulations, we measure the spectral index to be  $\nu \simeq 2$ .

## II. SETUP AND FORMALISM

We will carry out a numerical study of nonabelian, classical Yang-Mills theory coupled to an anisotropic bath of high momentum particles. The numerical tools were already presented in detail in [12], and this paper is a continuation of that work. To make our presentation more self-contained, we will briefly review the setup and formalism here.

Our treatment is founded on two assumptions about the system under study. The first is that the coupling  $\alpha_s \ll 1$ . The second is that there is a separation of scales between the momentum of the typical excitation,  $p$ , and the *screening scale*  $k \ll p$ . The screening scale is set by the momentum  $p$  and number density  $n$  of the typical excitations as  $k^2 \sim g^2 n/p$ . The number density is given by  $n = \int_{\mathbf{p}} f_{\mathbf{p}} \sim p^3 \bar{f}_p$ , where  $f_{\mathbf{p}}$  is the occupancy of momentum state  $\mathbf{p}$  and  $\bar{f}_p$  is its angular average. Therefore there is a scale separation  $k \ll p$  provided that the angular-averaged occupancy  $\bar{f}_p$  of typical excitations is  $\ll 1/g^2$ . This is essentially a diluteness condition on the typical excitations in the system.

In the context of heavy ion collisions, the condition  $\alpha_s \ll 1$  is formally valid for the collision of extremely large and high-energy heavy ions [6, 15]. The initial angular-averaged occupancy is at most  $\bar{f}_p \sim 1/g^2$ , which is the saturation limit [6, 15]<sup>1</sup> (corresponding to

---

<sup>1</sup> If the initial occupancies were  $\gg 1/g^2$ , then the magnetic screening length they would provide would be

number and energy densities  $n \sim p^3/g^2$  and  $\epsilon \sim p^4/g^2$ ). The density  $n$  of the original particles, and so  $\bar{f}_p \sim n/p^3$ , will fall with time as the system expands. So the scale separation condition  $\bar{f}_p \ll 1/g^2$  will be satisfied at least for  $\tau \gg \tau_0$  (up until the much later time when the particles of momentum  $p$  lose their energy and the plasma thermalizes—see, for example, the discussion in the original bottom-up scenario of Ref. [6]).

If we have a clean separation between the screening scale  $k$  and typical momenta  $p$ , then we can describe the physics on length scales  $x \sim 1/k$  in terms of (i) classical fields with wave vectors  $\sim k$  and (ii) a distribution of classical particles (possessing well defined momenta and positions) representing excitations with momenta  $\sim p$ . This is a Vlasov equation treatment. With a little more work [12, 16, 17], one may work in terms of a classical field variable  $A_\mu^a(\mathbf{x})$ , a variable  $W^a(\mathbf{v}, \mathbf{x})$ , which represents the net (adjoint) color of all particles moving in direction  $\mathbf{v}$  at point  $\mathbf{x}$ , and a background colorless particle density with angular distribution  $\Omega(\mathbf{v}, \mathbf{x})$  and polarizability characterized by a screening mass  $m^2$ ,

$$m^2 = \sum g^2 t_r \int \frac{d^3 p}{(2\pi)^3 p^0} f(\mathbf{p}), \quad (2.1)$$

with the sum over spin and particle type (including anti-particles).<sup>2</sup> Here  $t_r$  is a color group factor [defined in terms of color generators  $T$  by  $\text{tr}(T^a T^b) = t_r \delta^{ab}$  and equal to 3 for gluons]. For an isotropic medium,  $m^2 = \frac{1}{2} m_D^2 = \frac{3}{2} \omega_{\text{pl}}^2$ , where  $m_D$  is the Debye mass and  $\omega_{\text{pl}}$  is the plasma frequency.

We argued in [5] that the intrinsic length and time scales for the instability to develop are short compared to the length and time scales on which the heavy ion system as a whole evolves. Therefore we will restrict our attention in this (still somewhat exploratory) study to a non-expanding system with spatially uniform  $\Omega(\mathbf{v})$ . The evolution equations for  $A_\mu$  and  $W$  are

$$D_\nu F^{\mu\nu}(\mathbf{x}) = \int_{\mathbf{v}} v^\mu W(\mathbf{v}, \mathbf{x}), \quad (2.2)$$

$$(D_t + \mathbf{v} \cdot \mathbf{D}_x) W = m^2 [\mathbf{E} \cdot (2\mathbf{v} - \nabla_v) + \mathbf{B} \cdot (\mathbf{v} \times \nabla_v)] \Omega(\mathbf{v}). \quad (2.3)$$

The first equation is the Yang-Mills field equation, with  $W(\mathbf{v})$  giving rise to a current. The second equation, derived in Ref. [12], shows how electric and magnetic fields can polarize the colorless distribution of particles to create a net color moving in each direction. The dynamics of the soft fields is equivalent to that of hard-loop effective theory [18].

For a fully nonperturbative study of this system, we implement these equations on a lattice. The treatment of the classical, Minkowski space gauge fields on the lattice is the standard one [19]. The representation of the  $W$  fields is developed in [12, 17] and consists of replacing first derivatives with forward-backwards (covariantized) differences in Eq. (2.3), and expanding the space of velocities  $\mathbf{v}$  in spherical harmonics, truncated at a finite but large  $\ell_{\text{max}}$ . In this work we make one additional modification which improves approach to the  $\ell_{\text{max}} \rightarrow \infty$  limit and so reduces the memory and time requirements for simulations: We

---

larger than the imputed typical momentum. However, the concept of momentum for an excitation of a gauge dependent field is only well defined and robust under gauge fixing prescriptions to an accuracy set by the magnetic screening length. These ideas are central to the idea of the saturation scale. However this argument does not depend on the saturation scenario as such.

<sup>2</sup> In previous work we have referred to  $m$  as  $m_\infty$ , but here we will drop the subscript.

apply a weak damping term to the large  $\ell$  spherical harmonic components of the  $W$  field. The reason this is an improvement is that very large  $\ell$  excitations of the  $W$  field tend to cascade to still larger  $\ell$ , due to the  $\mathbf{v} \cdot \mathbf{D}$  term in Eq. (2.3).<sup>3</sup> With a finite  $\ell_{\max}$  cutoff, some of this excitation energy “bounces off” the  $\ell_{\max}$  cutoff and re-enters the infrared. This effect becomes smaller as  $\ell_{\max}$  is raised, but can be largely eliminated with the damping term we add. This point is discussed and justified in greater detail in appendix A.

The goal of this paper is to understand the behavior of a would-be unstable system after the unstable modes have already grown to have nonperturbative occupancy. In the context of a heavy ion collision, this is probably the only relevant question; since the exponential growth rate is larger than the inverse system age for all times after the formation time of the plasma, there has always been time for unstable gauge field modes to grow to nonperturbative size. Therefore we will begin our system with initial conditions for which the infrared (IR) fields are already nonperturbatively large. Again, since this is a qualitative exploratory work, we will work in SU(2) rather than SU(3) gauge theory and we will only consider a single anisotropic particle distribution, the same as the one considered in Ref. [12].

In addition to our focus on large rather than small initial conditions, there are slight technical differences in our choice of initial conditions compared to those of Ref. [12]. We start the system with vanishing  $E$  and  $W$  fields and with the  $A$  field selected from the thermal ensemble at temperature  $T = 2m/g^2$ , but then field-smear to a scale  $1/2m$ .<sup>4</sup> This is a gauge-invariant procedure which corresponds perturbatively to multiplying a thermal spectrum for  $A(k)$  by  $\exp(-k^2/4m^2)$ . We will explain the field smearing procedure below because it also constitutes one of our best measurables for understanding, in a gauge-invariant fashion, what corresponds to infrared phenomena and what to ultraviolet.

### III. RESULTS: BEHAVIOR OF THE NONABELIAN CASCADE

Our first conclusion, already presented in our previous paper [12], is that the energy in soft electromagnetic fields grows linearly with time. This is displayed in Fig. 2, which shows that the linear behavior is common to electric and magnetic fields and is robust to changes in the lattice spacing. However, this result leaves it unclear whether or not this represents continued growth of the soft unstable fields, whether these fields “abelianize” [9], and whether they retain long time scale coherence. We now present evidence that the answer to all three questions is, “no.”

---

<sup>3</sup> The  $\mathbf{v} \cdot \mathbf{D}$  term mixes neighboring  $\ell$ 's because  $\langle \ell m | \mathbf{v} | \ell' m' \rangle$  has non-zero cases when  $\ell' = \ell \pm 1$ .

<sup>4</sup> In three dimensions, there should be no important qualitative difference between using a smeared thermal distribution for the initial conditions, as here, or a smeared Gaussian noise distribution, as in Ref. [12]. We have checked this for a variety of properties, such as the rate of linear growth of energy with time. The reason we use a different procedure here than in Ref. [12] is inessential, having to do with the development of our code.

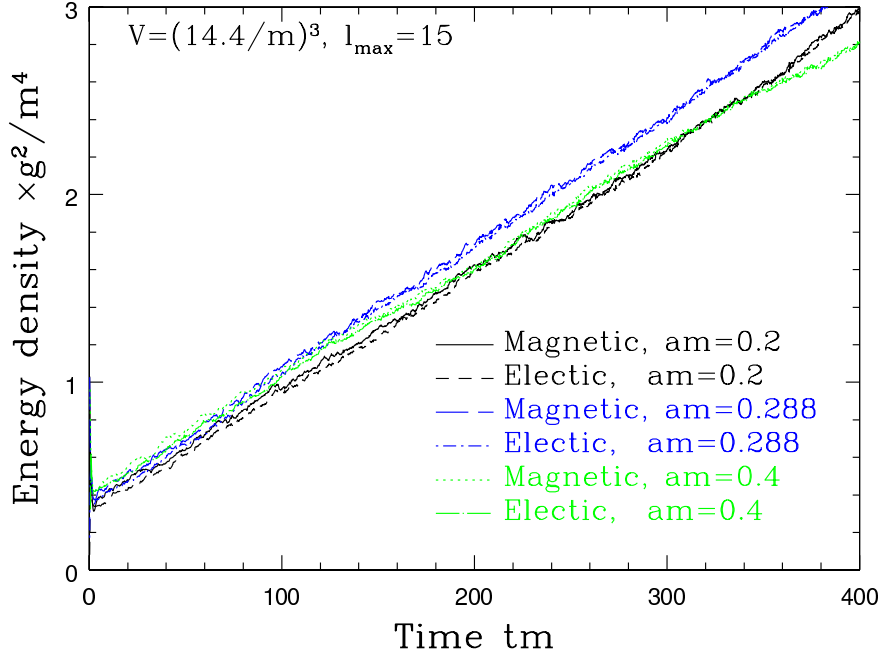


FIG. 2: (color online) Magnetic energy density  $\int d^3x B^2/2V$  and electric energy density  $\int d^3x E^2/2V$  as a function of time, for three lattice spacings of  $am = 0.2, 0.288, \text{ and } 0.4$ . After a brief transient owing to our choice of initial conditions, the electromagnetic energy rises linearly with time.

### A. Chern-Simons diffusion and IR dynamics

First, consider the behavior of Chern-Simons number,

$$N_{\text{CS}}(t) - N_{\text{CS}}(0) \equiv \int_0^t dt' \int d^3x \frac{g^2}{8\pi^2} \mathbf{E}^a(x, t') \cdot \mathbf{B}^a(x, t'). \quad (3.1)$$

Chern-Simons number is useful because it characterizes nonperturbative physics. In an abelian theory, or a nonabelian theory where the fields are weak,  $N_{\text{CS}}$  may fluctuate about zero but cannot drift away from zero permanently. That is because permanent change requires topology change (the Minkowski version of instantons). Therefore, ignoring small fluctuations, the time evolution of  $N_{\text{CS}}$  is purely indicative of the dynamics of nonperturbatively large fields. Fully topological algorithms for tracking  $N_{\text{CS}}$  in a real-time gauge field evolution already exist. We use the one from Ref. [20], which is a modification of a technique due to Ambjørn and Krasnitz [21].

A sample Chern-Simons number trajectory, from the  $am = 0.2$  evolution shown in Fig. 2, is shown on the left in Fig. 3. Chern-Simons number is changing by large amounts (indicating nonperturbatively large fields), and in a chaotic fashion (indicating that the fields have no long time-scale stability). This means that the soft fields remain large, but evolve dynamically, changing on a time scale set by the scale  $m^{-1}$ . To see this better, consider the auto-correlator  $\langle \dot{N}_{\text{CS}}(t + \Delta t) \dot{N}_{\text{CS}}(t) \rangle$ , shown on the right in that figure. This correlator indicates over what time scale coherent changes to the gauge fields occur. The figure presented represents an average over time and over 10 independent initial conditions drawn from the same ensemble, using a  $50^3$  lattice with  $am = .288$  and  $\ell_{\text{max}} = 15$ . The errors were determined by the jackknife method.

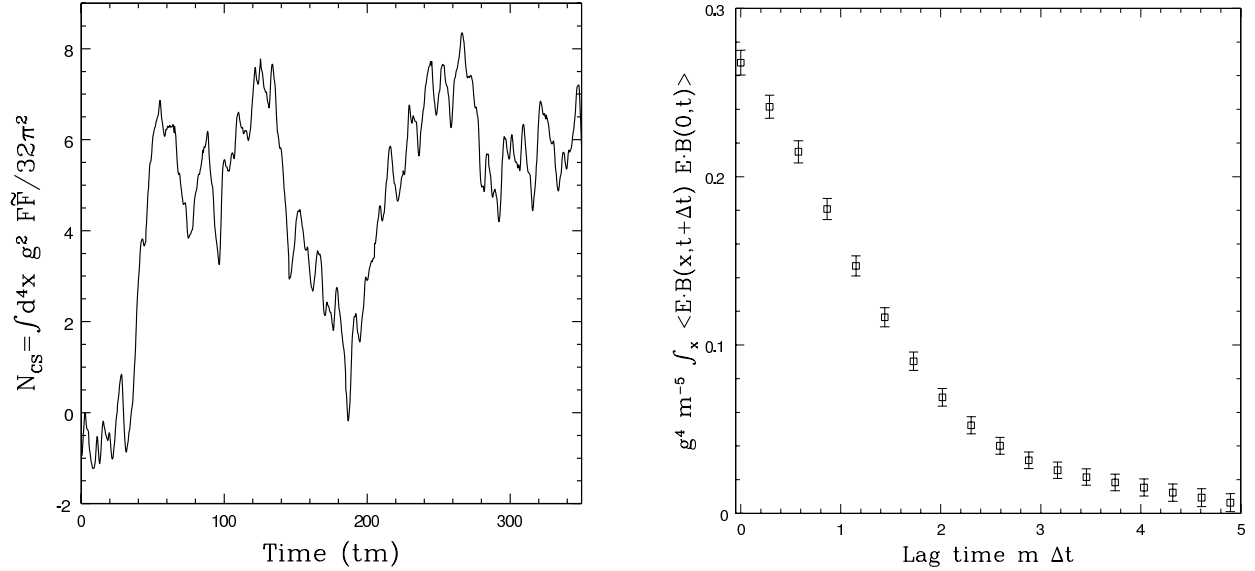


FIG. 3: *Left*: typical  $N_{\text{CS}}$  evolution in the linear regime. *Right*: the autocorrelator  $\dot{N}_{\text{CS}}\dot{N}_{\text{CS}}$ , or  $\int_x \langle (E \cdot B)[0, t](E \cdot B)[x, t + \Delta t] \rangle$ , as a function of lag time  $\Delta t$ . Chern-Simons number changes randomly with coherence time scale of order  $m^{-1}$ . The measurements were made on spatially smeared copies of the fields, as described in [20], with smearing extent  $\tau = 0.16/m^2$ . (*left*:  $72^3$  lattice,  $am = 0.2$ ,  $\ell_{\text{max}} = 15$ ; *right*:  $50^3$  lattice,  $am = 0.288$ ,  $\ell_{\text{max}} = 15$ )

Although we have not shown it in the figure, we have also checked that the evolution of  $N_{\text{CS}}$  does not speed up or slow down during the course of the linear rise in magnetic energy. For instance, comparing the first and second halves of the evolutions used to make Fig. 3, the Chern-Simons number diffusion rate (sphaleron rate) is consistent between the two halves to within 10% error bars, and the full auto-correlator is also consistent within errors. What this tells us is that the IR fields truly are nonperturbative, that they evolve with a characteristic time scale of order  $1/m$ , and that the time scale and the size of the nonperturbative fields is constant throughout the linearly growing regime.

## B. Coulomb gauge spectra

If IR fields are not growing, then the linear growth of magnetic energy must reflect growth of higher-momentum modes of the soft gauge field. To clarify the situation, it would be useful to know the power spectrum of the soft gauge fields as a function of wavenumber  $k$  and time  $t$ . We will start with a direct but gauge-dependent measurement of the power spectrum in Coulomb gauge. Later we will discuss how the spectrum can be accessed indirectly through gauge-invariant measurement involving smearing (also known as cooling) of the field configurations.

Our picture (to be supported by data below) is that, during the linear growth phase of the total energy in soft fields, the soft fields consist of (i) a non-perturbative IR component plus (ii) a perturbative component in the form of higher-momentum plasmons. We would like to know the distribution function  $f(k)$  of these plasmons as a function of  $k$ . We fix Coulomb gauge using the standard algorithm [22] adopted to the real-time case [23]. Then we (i) extract the Fourier spectrum of  $\mathbf{A}$  and  $\mathbf{E}$ , (ii) evaluate the two point function,

averaging over  $\mathbf{k}$  vectors in narrow blocks of  $|\mathbf{k}^2|$ ,<sup>5</sup> and (iii) define the distribution function as determined by  $\mathbf{A}$  and as determined by  $\mathbf{E}$  through<sup>6</sup>

$$\begin{aligned} f_A(k) &\equiv \frac{k}{N_{\text{dof}}V} \langle \mathbf{A}^2(k) \rangle, \\ f_E(k) &\equiv \frac{1}{N_{\text{dof}}kV} \langle \mathbf{E}^2(k) \rangle. \end{aligned} \quad (3.2)$$

Here,  $V$  is the total spatial volume and

$$N_{\text{dof}} = 6 \quad (3.3)$$

accounts for the two transverse polarization states and the  $3 = N_c^2 - 1$  adjoint color states in SU(2) gauge theory.

On scales where the fields are nonperturbatively large, these distribution functions are difficult to interpret, depending somewhat on the gauge fixing procedure. We do not expect  $f_A$  to equal  $f_E$ ; indeed, if the dominant fields are slowly evolving or unstable magnetic fields, we expect  $f_A > f_E$ , perhaps by a large margin. On scales, presumably at larger  $k$ , where the fields are perturbative, we should see  $f_A \simeq f_E$  if the relevant degrees of freedom are behaving as plasmons with  $k > m$ . Therefore, the ratio  $f_A/f_E$  serves as a diagnostic of whether the physics is nonperturbative and whether the degrees of freedom are primarily independently propagating plasmons or something else, such as the magnetic fields associated with hard particle currents.

To test this, we evolved the system for a time of  $mt = 400$  in a  $64^3$  box with  $\ell_{\text{max}} = 15$  and lattice spacing  $am = 0.25$ , corresponding to a (large) physical volume of  $(16/m)^3$ , tracking the distribution functions after the initial transient had died and the magnetic field energy was undergoing linear growth. The occupancy after initial transients is displayed on the left in Fig. 4, showing that, as expected, the IR has nonperturbatively large fields, while fields are perturbative at larger wave number. On the right in the figure, we show the time development. Each curve is time-averaged over an interval of  $\Delta t = 12.5/m$ , and the central times of consecutive curves are spaced apart by  $25/m$ . The IR occupancies remain nonperturbative but with stable amplitude, while the UV occupancy increases. At any  $k$ , the occupancy rises and eventually saturates; the saturation point progresses to larger  $k$ . This looks like a momentum-space (kinetic) cascade.

Cascades of energy from the infrared to the ultraviolet are familiar from turbulence in hydrodynamics and from many other physical systems. There are also weakly coupled examples such as weak plasma turbulence in traditional plasma physics [24], and theoretical studies of post-inflationary thermalization in the early universe [25]. Such cascades typically lead to a steady-state, power law distribution for the power spectrum  $f(k)$ , usually referred to as a Kolmogorov spectrum (in honor of the application to hydrodynamic turbulence). Different microphysics leads to different powers of  $k$ . A thermal spectrum is  $f(k) \propto k^{-1}$ . Cascades in scalar field theories during ‘‘preheating’’ after inflation, for example, typically

<sup>5</sup> technically, we use the lattice  $\mathbf{k}^2$ ,  $\sum_i (4/a^2) \sin^2(k_i a/2)$ .

<sup>6</sup> Consider the total energy of a gas of weakly-interacting, high-momentum ( $k \gg m$ ) plasmons. This could be written in terms of  $f$  as  $N_{\text{dof}}V \int_{\mathbf{k}} \omega_k f_{\mathbf{k}} \simeq \int_{\mathbf{k}} k f_{\mathbf{k}}$  or in terms of the fields as  $N_{\text{dof}}V \int_{\mathbf{k}} \frac{1}{2} (E_{\mathbf{k}}^2 + B_{\mathbf{k}}^2)$ . Since  $E_{\mathbf{k}}^2 \simeq B_{\mathbf{k}}^2$  for such plasmons, and  $B_{\mathbf{k}}^2 \simeq k^2 A_{\mathbf{k}}^2$  in Coulomb gauge, we can also write the energy as  $\int_{\mathbf{k}} E_{\mathbf{k}}^2$  or  $\int_{\mathbf{k}} k^2 A_{\mathbf{k}}^2$ . Comparison of these expressions leads to the identification (3.2).



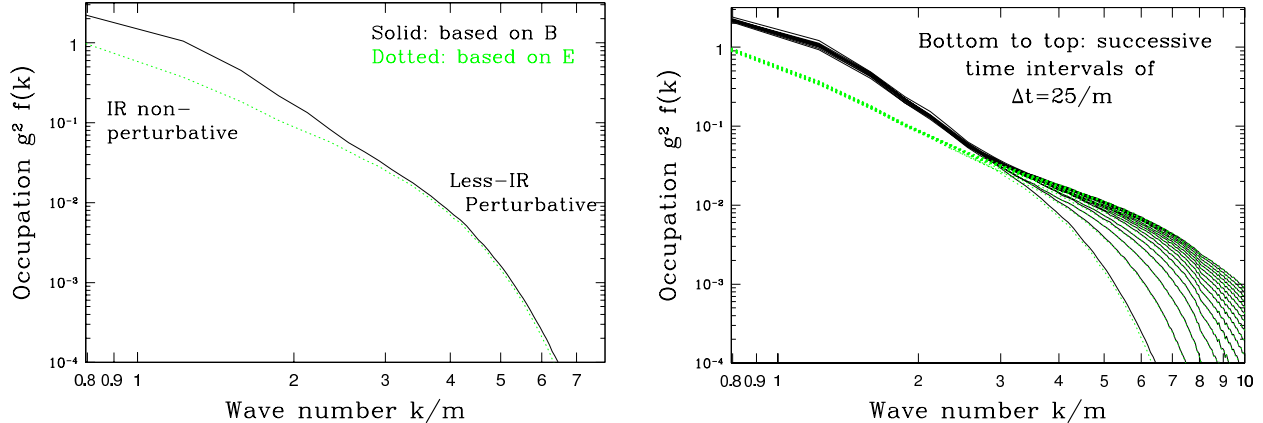


FIG. 4: (color online) Soft gauge field power spectra: *left*, initial; *right*, as a function of time. The IR fields are in a quasi-steady state, and the energy cascades towards more UV modes. ( $64^3$  lattice,  $am = 0.25$ ,  $\ell_{\max} = 15$ )

display a power spectrum with various power laws at different stages, such as  $f \propto k^{-3/2}$  and  $k^{-5/3}$  [25]. Obviously we do not expect power behavior at values of  $k$  where the field is nonperturbative; indeed, it is not even clear whether to use  $f_A$  or  $f_E$  in this region. However, we do expect power behavior for  $k$  large enough that  $f_A \simeq f_E$ , but small enough and at late enough times that  $f(k)$  has become nearly time independent.

The first figure in Fig. 5 repeats the righthand figure from Fig. 4 and shows that the cascade region is well fitted by a power law with  $f \propto k^{-2}$ . Unfortunately, the most ultraviolet wave numbers involved in the cascade are already at large enough  $k$  that lattice spacing effects may be a concern.<sup>7</sup> As a check on the robustness of the result, we performed a second evolution, also in a  $64^3$  box, with the same choice of  $\Omega(\mathbf{v})$ , but with  $am = 1/6$  rather than  $1/4$ , and going out to a time of  $mt = 800$ . The smaller spacing means that the physical volume was somewhat smaller. Nevertheless, it was large enough: we have checked agreement within errors of the  $N_{CS}$  diffusion coefficients, and close agreement in the energy growth rates. In any case the physics of the cascade is presumably more ultraviolet than the physics of the instability, and should not show severe volume sensitivity. The power spectrum from this evolution is shown on the right in Fig. 5, and is in very good agreement with the larger volume figure. The line superposed is drawn to guide the eye and is not actually a fit; it is precisely the same line in each figure.

We have found power-law fall-off  $f(k) = k^{-\nu}$  with spectral index  $\nu \simeq 2$ . To get a crude idea of the error in our determination of  $\nu$ , we show a more detailed view in Fig. 6 of the late-time distribution on the finer lattice. We show least-square fits of various power laws ( $\nu = 1.6, 1.8, 2.0, 2.2, 2.4$ ) to the data points<sup>8</sup> in the range  $3 < k/m < 8$ . The  $\nu = 2$  fit has the longest span of agreement, and we take our final result to be  $\nu = 2 \pm 0.2$ .

<sup>7</sup> For example, there is a small ripple in the first figure of Fig. 4 at  $k/m = 8$ . For  $am = 0.25$ , this is the lowest  $k^2$  value where the lattice group velocity can vanish, corresponding to a Van Hove singularity.

<sup>8</sup> We fit the  $f_E$  data. There is only a slight difference between  $f_E$  and  $f_A$ , which is at the IR end of the range chosen. The reason for slightly preferring  $f_E$  over  $f_A$  will become obvious in Sec. III C below.

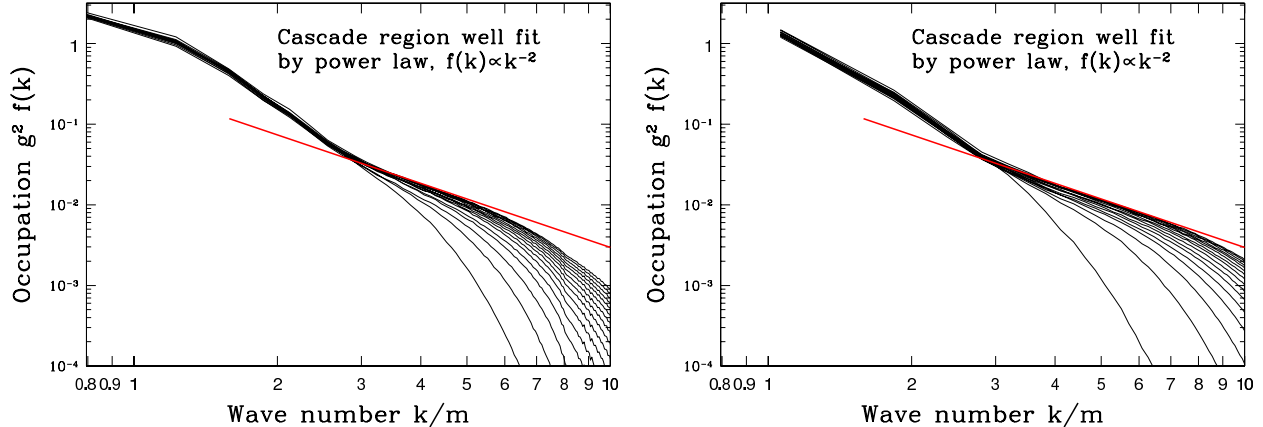


FIG. 5: (color online) *Left*: power spectrum as in Fig. 4, with a slope  $k^{-2}$  power law superposed to guide the eye. *Right*: same, but using a finer lattice spacing  $am = 1/6$  and twice as much physical time.

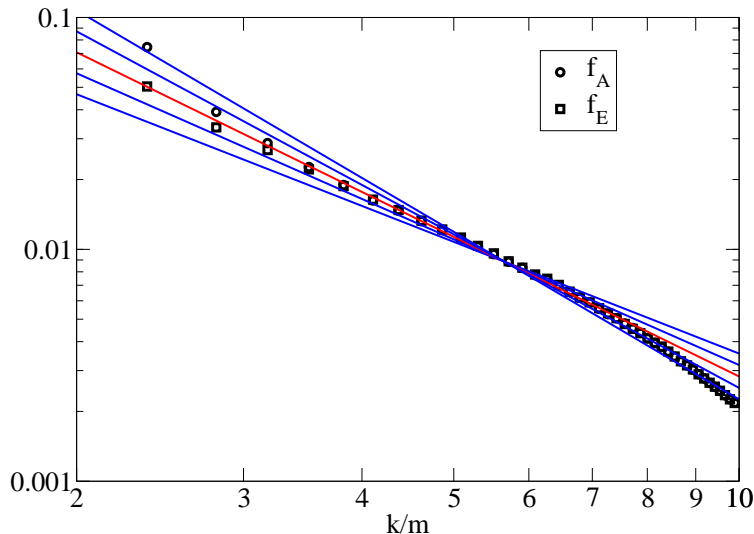


FIG. 6: (color online) The power-law region of the late-time Coulomb gauge distribution  $f$  shown fitted with lines corresponding to powers  $\nu = 1.6, 1.8, 2.0, 2.2,$  and  $2.4$ . The distribution functions are from the long-time, finer-lattice simulation shown in the right-hand plot of Fig. 5, averaged over  $700 \leq mt \leq 800$ . Each data point represents the center of one of the bins in  $k^2$  used to construct averages in (3.2). ( $64^3$  lattice,  $am = 1/6$ ,  $\ell_{\max} = 15$ )

### C. Gauge-invariant cooling

We argued that the Coulomb gauge spectrum of Fig. 5 should be trustworthy away from the IR because the higher-momentum components of the field are perturbative (as can be seen from the figures by the drop of occupation number with increasing momentum). However, in order to be sure that results are not artifacts of gauge fixing, it is usually preferable to investigate gauge theories with gauge-invariant observables. It is possible to probe aspects of power spectra in a gauge-invariant way by calculating the energy of smeared (also known as cooled) gauge fields. Smearing is a gauge-covariant process which

is a function of a parameter  $\tau$  known as the smearing depth. Define  $\mathbf{A}(t, \mathbf{x}; \tau=0)$  to be the actual gauge-field configuration  $\mathbf{A}(t, \mathbf{x})$  at a given physical time  $t$ . Then evolve in  $\tau$  according to

$$\frac{dA_i}{d\tau} = -\frac{\partial(B^2/2)}{\partial A_i} = D_j F_{ji}. \quad (3.4)$$

Here  $D$  is the covariant derivative and  $F$  is the field strength, also using the smeared field  $\mathbf{A}(t, \mathbf{x}; \tau)$ . This is a gauge-invariant procedure which has a straightforward lattice implementation. Such smearings have a long history in lattice gauge theory studies; for instance they are also used extensively in our technique for measuring  $N_{\text{CS}}$ . Other fields can also be smeared. For instance, we define a smeared  $W$  field through,

$$\partial_\tau W(\mathbf{x}, \mathbf{v}; \tau) = D^2 W(\mathbf{x}, \mathbf{v}, \tau), \quad (3.5)$$

where again  $D^2$  is the covariant derivative using the smeared gauge field at the same smearing depth  $\tau$ . Note that we do not introduce smearing into the dynamical evolution of the fields in time ( $t$ ); we only use smearing for making measurements. To answer the question “what is the smeared  $B^2$  at time  $t$ ?”, we make a copy of the fields at time  $t$ , apply smearing, and measure  $B^2$  on it.

Smeared fields are good at telling us whether the energy going into soft electromagnetic fields is appearing in very long wavelength, nonperturbative fields, or in plasmons with larger wave number. To study this, we consider the magnetic field energy density  $B^2/2$  as a function of time and of smearing depth, shown in Fig. 7. Very roughly, smearing to a depth  $\tau$  eliminates fields with  $k^2 > (2\tau)^{-1}$  and leaves fields with smaller  $k$ . But near  $k^2 \sim (2\tau)^{-1}$ , the fields are only partially removed, so the real story is slightly more complicated; smearing is similar to a Laplace transform of the power spectrum with  $k^2$  playing the role of time. The figure shows that the infrared energy is stable through the evolution. (It bounces around, which shows that the fields are evolving and that it is a small number of degrees of freedom contributing to the infrared energy. This bouncing would average out in larger volumes because of incoherent averaging.) The total energy ( $\tau=0$ ) rises linearly.

Based on the cascade picture of Fig. 5, what behavior should we have expected for the intermediate case of moderate  $\tau$ ? For any fixed smearing  $\tau$ , the energy should eventually stop growing once the modes with  $k^2 \lesssim \tau$  have grown to reach their steady-state distribution in the cascade. The smaller  $\tau$ , the longer it should take to reach the steady state. The  $m^2\tau = 4/256$  curve in Fig. 7 is a good example of an initial rise in energy that then tapers off and is plausibly approaching a steady-state value. It is unclear from our data whether the smaller (non-zero)  $\tau$  curves will eventually reach steady-state values. The problem is that cooling does not select out a single  $k$  but gives a superposition in the form of a Laplace transform. Note, for instance, that the  $k^{-2}$  behavior of the Coulomb spectrum of Fig. 4 is limited to the relatively narrow range of  $3 \lesssim k/m \lesssim 5$ . With infinite computing resources, one could run long enough, on fine enough lattices, to extend this region over a huge range of  $k$ , and then one would expect to see the predicted behavior in Fig. 7 for a wide range of  $\tau$ .

But there is a way to check that our Coulomb gauge results are trustworthy. We can Laplace transform the Coulomb gauge spectrum and see if it agrees with the (gauge-invariant) smeared measurements of Fig. 7. Perturbatively, the smeared magnetic energy density should be related to the distributions  $f(k)$  by

$$\mathcal{E}_B(\tau) = \frac{N_{\text{dof}}}{2} \int \frac{d^3k}{(2\pi)^3} k f(k) e^{-2k^2\tau}. \quad (3.6)$$

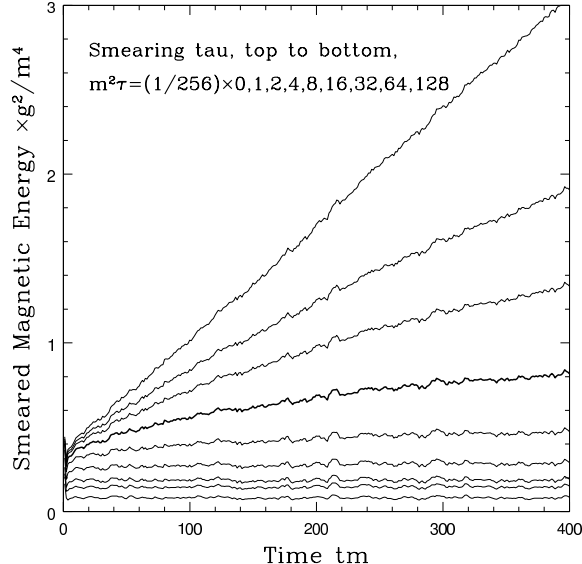


FIG. 7: Magnetic energy density as a function of time and smearing depth. ( $64^3$  lattice,  $am = 0.25$ ,  $\ell_{\max} = 15$ )

Note that the growth of  $d^3k \times k \sim k^3 dk$  with  $k$  typically more than compensates for the fall of  $f(k)$  with  $k$  in Fig. 5, so that these integrals are dominated by  $k^2 \sim \tau^{-1}$  at late times  $t$ . We replot Fig. 7 in Fig. 8, superposed with dashed lines that show the results of (3.6) with  $f = f_E$ . The results are very close until one cools deep into the infrared. (We also show one sample curve based on  $f_A$ , which gives slightly less accurate results than  $f_E$ . The  $f_A$  have a more significant IR contribution than  $f_E$ , as can be seen in Fig. 4.) We conclude that Coulomb-gauge distributions provide a reasonably accurate description of the physics of the cascade far from the IR, supporting our conclusions based on Figs. 4 and 5.

The instability preferentially excites gauge fields with  $\mathbf{k}$  vector along the  $z$  axis (the axis about which the particle momentum distribution is oblate) [5, 8]. Such modes have primarily transverse magnetic fields, so  $B_z^2 \ll B_x^2 + B_y^2$  for the fields excited by the instability. Therefore we might expect this behavior of the infrared gauge fields. If the higher momentum fields represent a nearly thermalized bath, they will be close to isotropic and the ratio  $B_z^2/(B_x^2 + B_y^2)$  will be 1/2. But if they scatter predominantly off the IR fields, they may also carry a momentum space anisotropy. To study this, Fig. 9 shows the ratio  $B_z^2/(B_x^2 + B_y^2)$  as a function of smearing, for the same lattice parameters as in Fig. 7. Indeed, the soft fields are anisotropic as expected. The unsmearred fields are (on average) less so, but still have a definite anisotropy along the  $z$  axis.

The picture that has emerged is that there are soft, anisotropic, nonperturbatively large gauge fields with higher wave-number plasmons superposed. The size of the soft gauge fields fluctuates about a steady mean, and the plasmons become more numerous, populating higher and higher wave numbers. One way to check whether the interpretation of the high wave number excitations as plasmons is correct, is to look at the  $W$  fields. We will concentrate on the  $\ell = 1$  component of  $W$ , which is the same as the particle current up to a factor:  $j^2 = (1/3) \sum_m W_{1m}^2$  [12]. A plasmon with  $k \gg m$  carries almost all its energy in  $E^2$  and  $B^2$ , roughly equipartitioned, and only a subdominant amount in currents. Therefore, if the energy growth really represents a growing number of plasmons with  $k > m$ , then  $\langle j^2 \rangle$  should grow slowly if at all, and should be IR dominated. Fig. 10 shows our measurements,

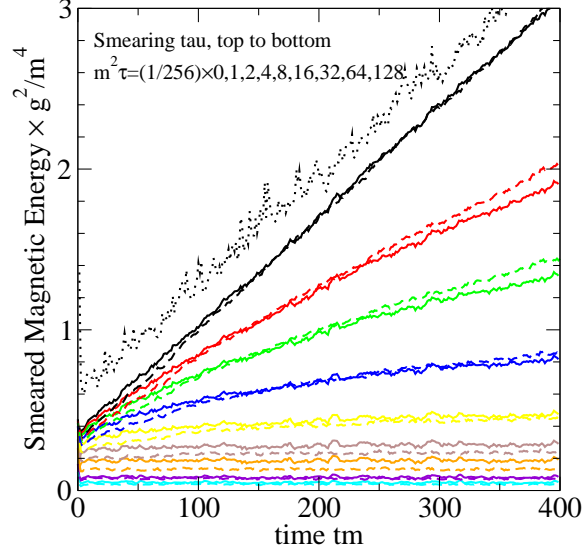


FIG. 8: (color online) The solid lines are the same as Fig. 7. The dashed lines represent the corresponding results extracted from the Coulomb-gauge spectra  $f_E$  of Fig. 4. The single dotted line at the top shows a similar extraction of the unsmearing ( $\tau=0$ ) curve from  $f_A$  instead of  $f_E$ . The noisy difference with the corresponding  $f_E$  curve is an IR effect, and this difference remains until one cools substantially (not shown). ( $64^3$  lattice,  $am = 0.25$ ,  $\ell_{\max} = 15$ )

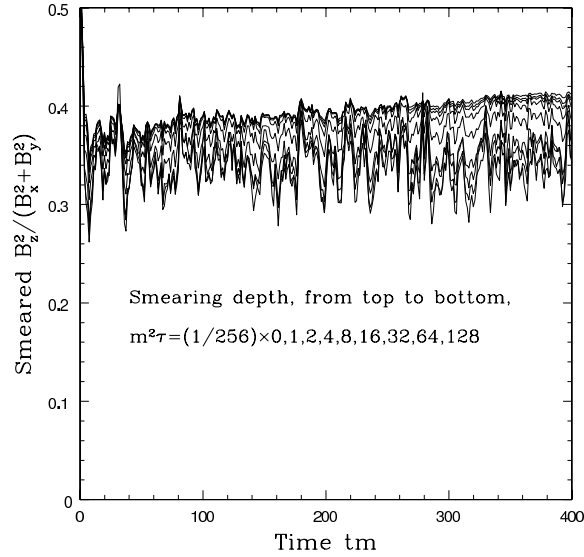


FIG. 9: The ratio  $B_z^2/(B_x^2+B_y^2)$  as a function of time and smearing depth. ( $64^3$  lattice,  $am = 0.25$ ,  $\ell_{\max} = 15$ )

and the lack of growth with time is clear.<sup>9</sup> [Following Ref. [12], we have normalized the

<sup>9</sup> In contrast, a slight growth of current can be seen at very late times in Fig. 11 of Ref. [12]. This growth appears to be a late-time artifact of the undamped treatment of  $\ell_{\max}$  in that reference, as we discuss in the appendix.

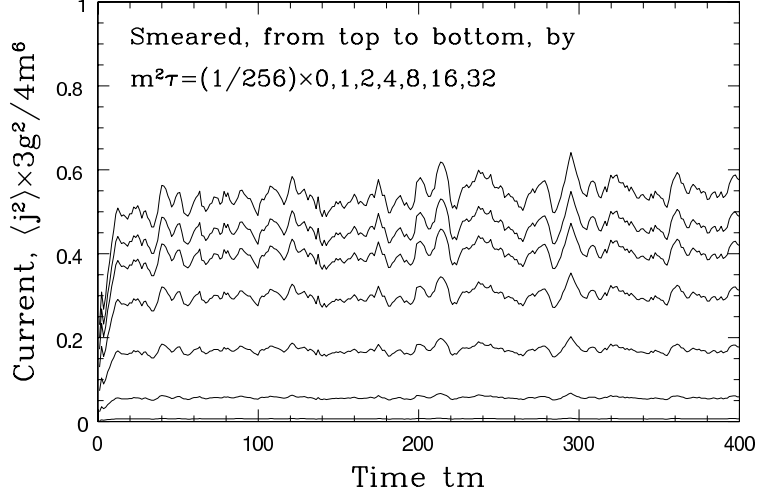


FIG. 10: Current squared as a function of time and cooling depth. The current remains predominantly infrared, and shows large fluctuations about a nearly flat trend through the evolution. ( $64^3$  lattice,  $am = 0.25$ ,  $\ell_{\max} = 15$ )

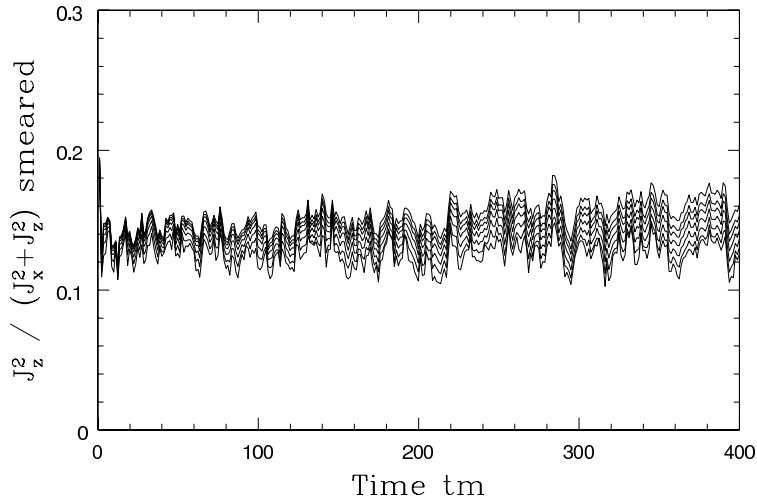


FIG. 11: The ratio of  $j_z^2$  to  $j_x^2 + j_y^2$  for the various cooling depths of Fig. 10. Note the scale of the vertical axis. ( $64^3$  lattice,  $am = 0.25$ ,  $\ell_{\max} = 15$ )

curves by plotting  $(3/4m^2)j^2 = (1/4m^2)\sum_m W_{1m}^2$ , which is the contribution of the  $\ell=1$  components of  $W$  to what would be a conserved energy  $(E^2 + B^2)/2 + (1/4m^2)\sum_{\ell m} W_{\ell m}^2$  for isotropic systems.]  $j^2$  falls more slowly with cooling depth than the magnetic energy of Fig. 7, indicating less power in the ultra-violet. We also find, in Fig. 11, that  $j_z^2 \sim 0.13(j_x^2 + j_y^2)$ , nearly independent of time and smearing depth. A small ratio of  $j_z$  to  $j_x$  and  $j_y$  is expected if the currents are primarily associated with long wavelength, transverse modes in the directions which are perturbatively unstable.

## IV. DISCUSSION AND CONCLUSIONS

Putting our numerical results together, the physical picture which emerges is the following. Plasma instabilities drive IR gauge fields with  $k_z \gg k_\perp$  to grow. Nonperturbatively strong interactions between these soft field modes remove energy from these unstable modes, moving it instead into less-IR gauge field modes. The size of the soft nonperturbative fields reaches a quasi-steady state; if it grows larger, the nonperturbative physics removing energy gets more efficient, and if it gets smaller, the instability drives it back up. The energy absorbed via the instability from the hard particles thereby powers a cascade of soft gauge field excitation energy towards the ultraviolet. The cascade has power spectrum  $f(k) \propto k^{-\nu}$  with  $\nu \simeq 2$ . This is not a thermal spectrum, as also evidenced by the failure of  $B_z^2/(B_x^2+B_y^2)$  to approach  $\frac{1}{2}$ . We give a theoretical explanation of the value  $\nu = 2$  in another work [26].

These same instability-powered energy cascades should appear in the early stages of arbitrarily high-energy heavy ion collisions. These cascades will only be a temporary feature along the path to thermalization and will disappear by the time the plasma is finally fully thermalized. We leave to future work the complete integration of the physics of instabilities into quark-gluon plasma thermalization at arbitrarily high energies.

### Acknowledgments

We would like to thank Larry Yaffe for useful conversations, especially in the initial development of this project. This work was supported, in part, by the U.S. Department of Energy under Grant Nos. DE-FG02-97ER41027, by the National Sciences and Engineering Research Council of Canada, and by le Fonds Nature et Technologies du Québec.

### APPENDIX A: IMPROVING SIMULATIONS BY DAMPING HIGH $l$ MODES

In this appendix we argue that the large  $\ell_{\max}$  limit is achieved more quickly by applying weak damping on large  $\ell$  modes than by not doing so, and we present numerical evidence that this is the case.

At the perturbative level, the behavior of the isotropic version of the  $A$  and  $W$  field system has been investigated by Bödeker, Moore, and Rummukainen [17]. The correct analytic structure of the gauge field propagator in the presence of hard thermal loops (the infinite  $\ell_{\max}$ , isotropic theory) is that there should be a propagating “plasmon” pole at a frequency  $|\omega| > k$ , and a cut in the spectral weight for all frequencies  $|\omega| < k$ . Physically, the cut reflects Landau damping. It means that most of the energy of a long wavelength magnetic field should be absorbed by the particle degrees of freedom represented by the  $W$  fields, never to return. However, the finite  $\ell_{\max}$  system is a non-dissipative Hamiltonian system. Therefore it is not possible for it to contain cuts in the (leading order) propagator. Instead, the region which should contain the cut contains a series of poles and zeros in the propagator, illustrated in Fig. 12, which is taken from Ref. [17].

What this means is that the excitation energy present in the magnetic field, which is supposed to be Landau damped away, instead appears only in periodic oscillatory modes. Most of the energy is stored in the  $W$  fields, as is supposed to happen under Landau damping. However, a fraction of it periodically reappears as magnetic field energy, an effect which is unphysical. The size of this effect is determined by the number of  $W$  field modes,  $(\ell_{\max} + 1)^2$ ,

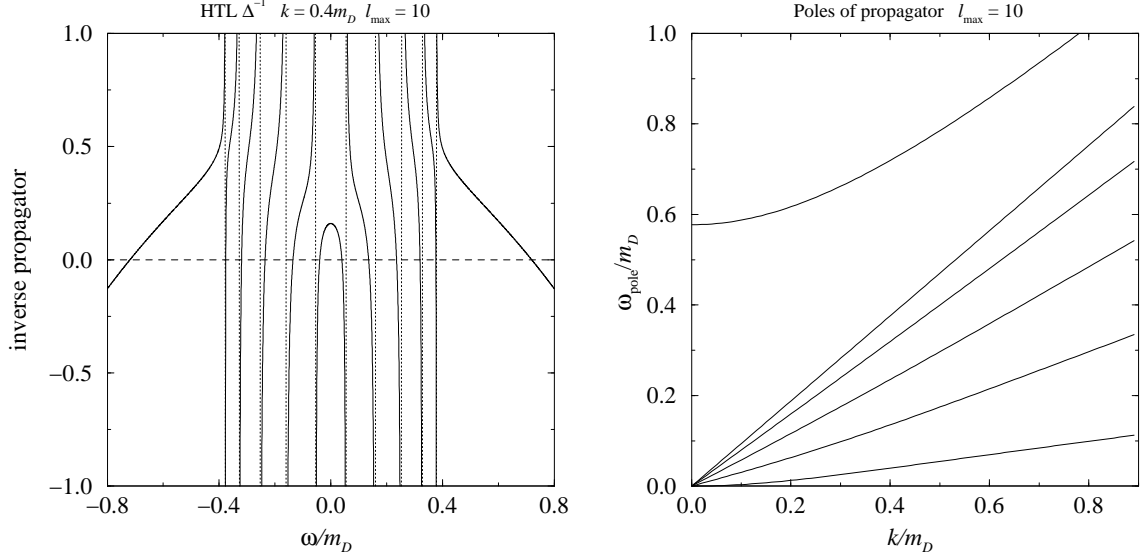


FIG. 12: *Left*: The inverse propagator with  $\ell_{\max} = 10$ , plotted against  $\omega/m_D$  with fixed  $k = 0.4 m_D$ . *Right*: The positive frequency poles of the propagator at  $\ell_{\max} = 10$ . In these figures, one can clearly see the development of the cut in the interval  $-k \leq \omega \leq k$ , and the two plasmon poles at  $\omega^2 \approx m_D^2/3 + 6k^2/5$ .

which sets the heat capacity of these modes to absorb and store excitation energy. The larger  $\ell_{\max}$  is, the more effectively the  $W$  fields can retain the energy rather than feeding it back to the magnetic fields.

The problem in the current context is that, in the anisotropic system, quite large amounts of  $W$  field excitation are generated. The derivative term  $\mathbf{v} \cdot \mathbf{D} W$  in Eq. (2.3) should cause this excitation energy to migrate to higher and higher  $\ell$  values. This is shown in the left-hand plot of Fig. 13, which shows how  $\sum_m W_{\ell m}^2$  varies with time and with  $\ell$ , if we start with large magnetic fields but with no initial excitation in the  $W$  fields. However, with a finite  $\ell_{\max}$  cutoff, the excitation cannot migrate to arbitrarily large  $\ell$ , as it should; some of it instead moves back into lower  $\ell$  and re-enters the gauge fields and small  $\ell$   $W$  fields. This causes a fake increase in the energy of these fields, which becomes more severe as  $\ell_{\max}$  is decreased.

Our approach to solve this problem is to assume that any excitation energy which reaches very large  $\ell$  values should continue to arbitrarily large  $\ell$  and be lost to the low  $\ell$  system. We can make this happen artificially by applying a damping term to the highest  $\ell$  modes, modifying the  $W$  equation of motion via

$$\frac{dW_{\ell m}}{dt} = (\text{previous}) - \gamma W_{\ell m} \Theta(\ell - \ell_{\text{damp}}). \quad (\text{A1})$$

That is, we add a term which causes exponential shrinkage with rate  $\gamma$  in all  $\ell$  at or above a cutoff  $\ell_{\text{damp}}$ . The damping should only affect the high  $\ell$  modes, so we choose  $\ell_{\text{damp}} = (2/3)\ell_{\max}$ . Note that the damping we apply is gauge invariant: so long as  $\ell_{\text{damp}} > 1$ , the current remains exactly conserved, because the current is determined by the  $\ell = 1$  modes and the charge density by  $W_{00}$ . We also have to choose a value for  $\gamma$ . If the value is too large, then the  $W$  fields with  $\ell > \ell_{\text{damp}}$  are effectively forced to be zero, which is equivalent to lowering  $\ell_{\max}$  to  $\ell_{\text{damp}}$ . Therefore we should choose  $\gamma < m$ , since  $m$  is the intrinsic scale



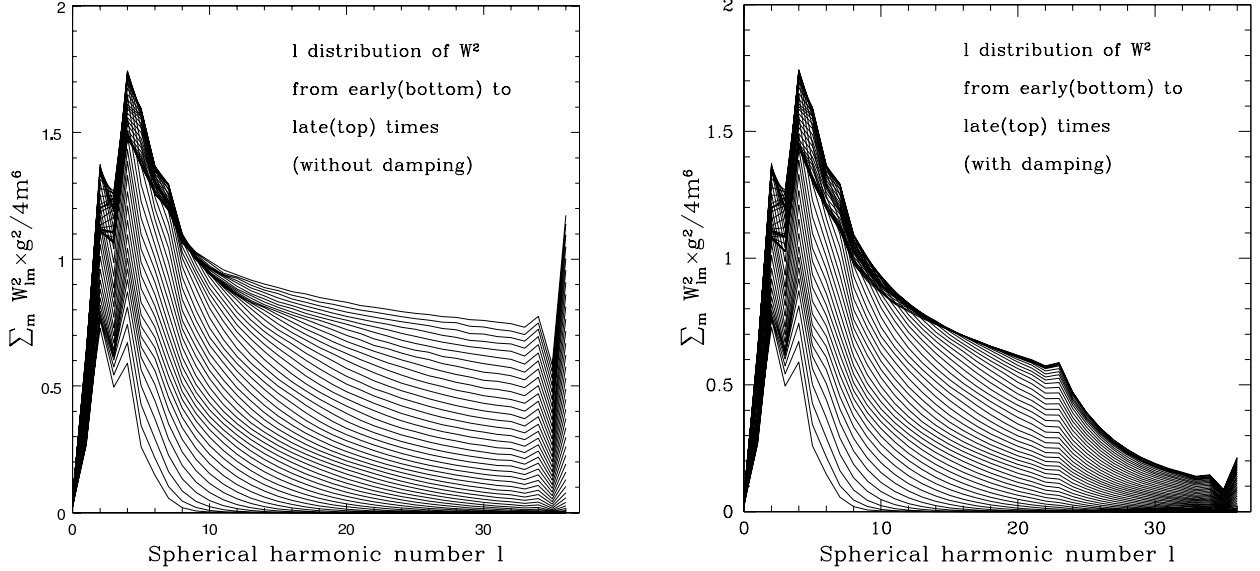


FIG. 13: Time and  $\ell$  dependence of  $\sum_m W_{\ell m}$  the amount of excitation in the  $W$  field. Each figure plots  $\sum_m W_{\ell m}$  against  $\ell$  at a series of time snapshots, for  $\ell_{\max} = 36$ . The left figure is without damping; the right figure has damping on  $\ell \geq 24$  modes. In each case, the time between successive lines is  $0.57/m$ . The two spikes at small  $\ell$  are the angular scales driven by the instability. The excitation introduced here cascades to larger  $\ell$ , eventually bouncing off the  $\ell_{\max}$  limit in the left figure but being absorbed at large  $\ell$  by the damping in the right figure. ( $50^3$  lattice,  $am = 0.288$ )

of the dynamics. We should also make sure we pick  $\gamma > m/\ell_{\max}$ ; otherwise the damping is too slow to do anything, as excitation energy can get from  $\ell_{\text{damp}}$  to  $\ell_{\max}$ , reflect, and go back below  $\ell_{\text{damp}}$  before being damped away. With this in mind, we have chosen  $\gamma = m/\sqrt{\ell_{\max}}$ .

Of course, it remains to test whether this procedure of damping large  $\ell$  modes really gives the same behavior as choosing an extremely large value for  $\ell_{\max}$  (which is numerically impractical, since the number of degrees of freedom rises as  $(1+\ell_{\max})^2$ ). To check, we have performed evolutions with the same initial random seed and other parameters but with different values of  $\ell_{\max}$ , and either with or without the damping term added. The results are shown in Fig. 14 for  $am = .288$ ,  $V = (14.4/m)^3$ , and the same  $\Omega(\mathbf{v})$  used in the main body of the paper [12]. On the left, we see magnetic energy growth vs. time. With and without damping, the growth rates converge (from opposite sides) towards the same large  $\ell_{\max}$  limit. But the damped results converge much faster: with damping, the magnetic energy growth does not change between  $\ell_{\max} = 15$  and  $\ell_{\max} = 24$ , and appears to coincide with the very large  $\ell_{\max}$ , undamped behavior. Now return to the flat result of Fig. 10 for the time dependence of  $j^2$ . On the right of Fig. 14, we see that this flat behavior is obtained only very gradually in the large  $\ell_{\max}$  limit unless damping is implemented, in which case it occurs immediately. For investigating current growth, damping is an essential numerical tool for practical simulations.

Naturally, if  $\ell_{\max}$  is too small, we will see errant behavior whether or not we implement damping. For the choice of  $\Omega(\mathbf{v})$  used here (*i.e.* for the degree of hard particle anisotropy in our simulations), Fig. 14 shows large deviation of the magnetic energy growth for  $\ell_{\max}$  below about 10. We have therefore conservatively used  $\ell_{\max} = 15$  for the bulk of the studies

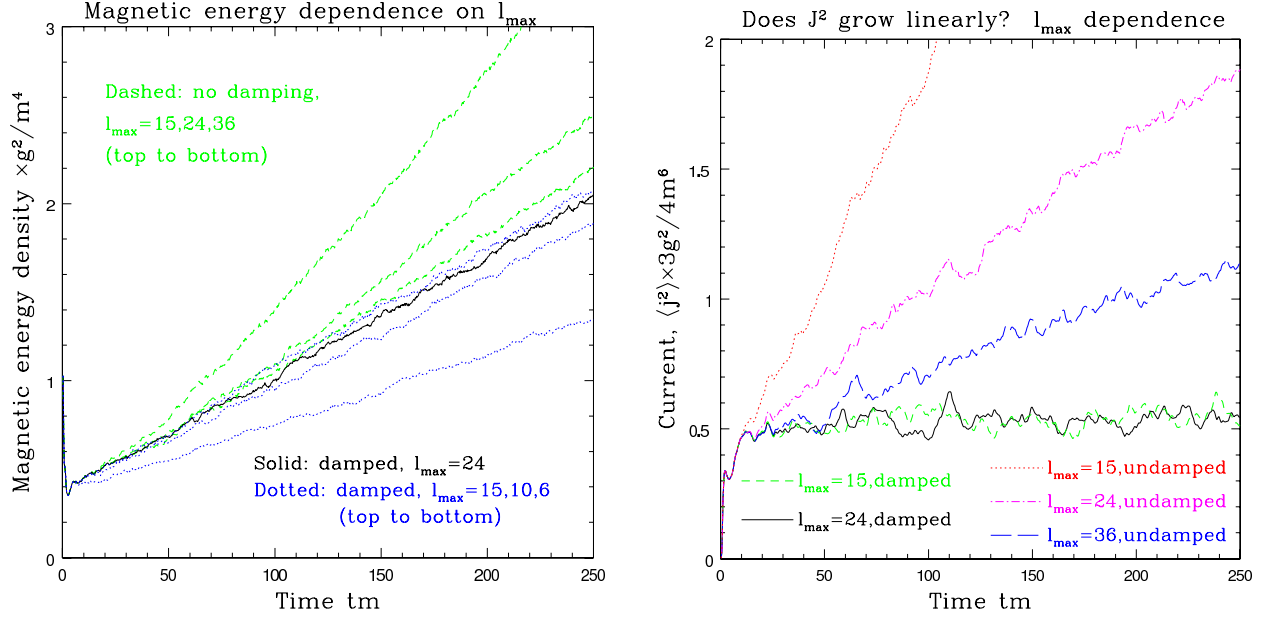


FIG. 14: (color online) *Left*: magnetic energy against time at different values of  $l_{\max}$ , with and without  $W$  damping. Without damping, the growth rate in  $B^2$  approaches a large  $l_{\max}$  value from above, approximately as  $1/(\ell_{\max}+1)^2$ . With damping, it approaches from below and obtains the large  $l_{\max}$  value much faster. *Right*: the same for  $\langle j^2 \rangle$ . The fact that this quantity does not grow is obtained immediately with damping, but only approached very slowly in the large  $l_{\max}$  limit without damping. ( $50^3$  lattice,  $am = 0.288$ )

presented in the main text.

- 
- [1] E. Shuryak, “Why does the quark gluon plasma at RHIC behave as a nearly ideal fluid?,” Prog. Part. Nucl. Phys. **53**, 273 (2004) [hep-ph/0312227]; M. Gyulassy and L. McLerran, “New forms of QCD matter discovered at RHIC,” Nucl. Phys. A **750**, 30 (2005) [nucl-th/0405013].
- [2] P. F. Kolb, P. Huovinen, U. W. Heinz and H. Heiselberg, “Elliptic flow at SPS and RHIC: From kinetic transport to hydrodynamics,” Phys. Lett. B **500**, 232 (2001) [hep-ph/0012137]; D. Teaney, J. Lauret and E. V. Shuryak, “Flow at the SPS and RHIC as a quark gluon plasma signature,” Phys. Rev. Lett. **86**, 4783 (2001) [nucl-th/0011058]; U. W. Heinz, “Thermalization at RHIC,” AIP Conference Proceedings **739**, *Hadron Physics and Relativistic Aspects of Nuclear Physics* (2004) 163 [nucl-th/0407067].
- [3] R. Baier, A. H. Mueller, D. Schiff and D. T. Son, Phys. Lett. B **539**, 46 (2002); D. Molnar and M. Gyulassy, Nucl. Phys. A **697**, 495 (2002) [Erratum-ibid. A **703**, 893 (2002)].
- [4] Z. Xu and C. Greiner, “Thermalization of gluons in ultrarelativistic heavy ion collisions by including three-body interactions in a parton cascade,” Phys. Rev. C **71**, 064901 (2005) [hep-ph/0406278].
- [5] P. Arnold, J. Lenaghan and G. D. Moore, “QCD plasma instabilities and bottom-up thermalization,” JHEP 08 (2003) 002 [hep-ph/0307325].
- [6] R. Baier, A. H. Mueller, D. Schiff and D. T. Son, “‘Bottom-up’ thermalization in heavy ion

- collisions,” *Phys. Lett. B* **502**, 51 (2001) [hep-ph/0009237].
- [7] S. Mrówczyński, “Stream instabilities of the quark-gluon plasma,” *Phys. Lett. B* **214**, 587 (1988); Y. E. Pokrovsky and A. V. Selikhov, “Filamentation in a quark-gluon plasma,” *JETP Lett.* **47**, 12 (1988) [*Pisma Zh. Eksp. Teor. Fiz.* **47**, 11 (1988)]; “Filamentation in quark plasma at finite temperatures,” *Sov. J. Nucl. Phys.* **52**, 146 (1990) [*Yad. Fiz.* **52**, 229 (1990)]; “Filamentation in the quark-gluon plasma at finite temperatures,” *Sov. J. Nucl. Phys.* **52**, 385 (1990) [*Yad. Fiz.* **52**, 605 (1990)]; O. P. Pavlenko, “Filamentation instability of hot quark-gluon plasma with hard jet,” *Sov. J. Nucl. Phys.* **55**, 1243 (1992) [*Yad. Fiz.* **55**, 2239 (1992)]; S. Mrówczyński, “Plasma instability at the initial stage of ultrarelativistic heavy ion collisions,” *Phys. Lett. B* **314**, 118 (1993); “Color collective effects at the early stage of ultrarelativistic heavy ion collisions,” *Phys. Rev. C* **49**, 2191 (1994); “Color filamentation in ultrarelativistic heavy-ion collisions,” *Phys. Lett. B* **393**, 26 (1997) [hep-ph/9606442].
- [8] P. Romatschke and M. Strickland, “Collective modes of an anisotropic quark gluon plasma,” *Phys. Rev. D* **68**, 036004 (2003) [hep-ph/0304092].
- [9] P. Arnold and J. Lenaghan, “The abelianization of QCD plasma instabilities,” *Phys. Rev. D* **70**, 114007 (2004) [hep-ph/0408052].
- [10] A. Rebhan, P. Romatschke and M. Strickland, “Hard-loop dynamics of non-Abelian plasma instabilities,” *Phys. Rev. Lett.* **94**, 102303 (2005) [hep-ph/0412016].
- [11] A. Dumitru and Y. Nara, “QCD plasma instabilities and isotropization,” *Phys. Lett. B* **621**, 89 (2005) [hep-ph/0503121].
- [12] P. Arnold, G. D. Moore and L. G. Yaffe, “The fate of non-abelian plasma instabilities in 3+1 dimensions,” *Phys. Rev. D* **72**, 054003 (2005) [hep-ph/0505212].
- [13] A. Rebhan, P. Romatschke and M. Strickland, “Dynamics of quark-gluon plasma instabilities in discretized hard-loop approximation,” hep-ph/0505261.
- [14] A. H. Mueller, A. I. Shoshi and S. M. H. Wong, “A possible modified ‘bottom-up’ thermalization in heavy ion collisions,” hep-ph/0505164; D. Bödeker, “The impact of QCD plasma instabilities on bottom-up thermalization,” hep-ph/0508223.
- [15] L. V. Gribov, E. M. Levin and M. G. Ryskin, “Semihard processes in QCD,” *Phys. Rept.* **100**, 1 (1983); J. P. Blaizot and A. H. Mueller, “The early stage of ultrarelativistic heavy ion collisions,” *Nucl. Phys. B* **289**, 847 (1987); L. D. McLerran and R. Venugopalan, “Computing quark and gluon distribution functions for very large nuclei,” *Phys. Rev. D* **49**, 2233 (1994) [hep-ph/9309289]; “Green’s functions in the color field of a large nucleus,” **50**, 2225 (1994) [hep-ph/9402335]; J. Jalilian-Marian, A. Kovner, L. D. McLerran and H. Weigert, “The intrinsic glue distribution at very small x,” *Phys. Rev. D* **55**, 5414 (1997) [hep-ph/9606337];
- [16] E. Iancu, “Effective theory for real-time dynamics in hot gauge theories,” *Phys. Lett. B* **435**, 152 (1998).
- [17] D. Bödeker, G. D. Moore and K. Rummukainen, “Chern-Simons number diffusion and hard thermal loops on the lattice,” *Phys. Rev. D* **61**, 056003 (2000) [hep-ph/9907545].
- [18] S. Mrowczynski, A. Rebhan and M. Strickland, “Hard-loop effective action for anisotropic plasmas,” *Phys. Rev. D* **70**, 025004 (2004) [hep-ph/0403256].
- [19] J. Ambjorn, T. Askgaard, H. Porter and M. E. Shaposhnikov, “Sphaleron Transitions And Baryon Asymmetry: A Numerical Real Time Analysis,” *Nucl. Phys. B* **353**, 346 (1991).
- [20] G. D. Moore, “Measuring the broken phase sphaleron rate nonperturbatively,” *Phys. Rev. D* **59**, 014503 (1999) [hep-ph/9805264].
- [21] J. Ambjorn and A. Krasnitz, “Improved determination of the classical sphaleron transition rate,” *Nucl. Phys. B* **506**, 387 (1997) [hep-ph/9705380].

- [22] J. E. Mandula and M. Ogilvie, “The Gluon Is Massive: A Lattice Calculation Of The Gluon Propagator In The Landau Gauge,” *Phys. Lett. B* **185**, 127 (1987).
- [23] G. D. Moore and N. Turok, “Lattice Chern-Simons number without ultraviolet problems,” *Phys. Rev. D* **56**, 6533 (1997) [hep-ph/9703266].
- [24] V. N. Tsytovich, *Lectures on Non-linear Plasma Kinetics* (Springer-Verlag, 1995).
- [25] D. T. Son, “Reheating and thermalization in a simple scalar model,” *Phys. Rev. D* **54**, 3745 (1996) [hep-ph/9604340]; R. Micha and I. I. Tkachev, “Turbulent thermalization,” *Phys. Rev. D* **70**, 043538 (2004) [hep-ph/0403101].
- [26] P. Arnold and G. D. Moore, in preparation.